Shared Molecular Targets Confer Resistance over Short and Long Evolutionary Timescales

Jing Li,[1] Ignacio Vázquez-García,[2,3,4,5] Karl Persson,[6] Asier González,[7] Jia-Xing Yue,[1] Benjamin Barré,[1] Michael N. Hall,[7] Anthony Long,[8] Jonas Warringer,[6] Ville Mustonen,[9] and Gianni Liti*[,1]

[1]Université Côte d'Azur, CNRS, Inserm, IRCAN, Nice, France

[2]Wellcome Trust Sanger Institute, Cambridge, United Kingdom

[3]Department of Applied Mathematics and Theoretical Physics, University of Cambridge, Cambridge, United Kingdom

[4]Department of Epidemiology and Biostatistics, Memorial Sloan Kettering Cancer Center, New York, NY

[5]Department of Statistics, Columbia University, New York, NY

[6]Department of Chemistry and Molecular Biology, University of Gothenburg, Gothenburg, Sweden

[7]Biozentrum, University of Basel, Basel, Switzerland

[8]Department of Ecology and Evolutionary Biology, University of California, Irvine, CA

[9]Organismal and Evolutionary Biology Research Programme, Department of Computer Science, Institute of Biotechnology, University of Helsinki, Helsinki, Finland

***Corresponding author:** E-mail: gianni.liti@unice.fr.

Associate Editor: Harmit Malik

Abstract

Pre-existing and de novo genetic variants can both drive adaptation to environmental changes, but their relative contributions and interplay remain poorly understood. Here we investigated the evolutionary dynamics in drug-treated yeast populations with different levels of pre-existing variation by experimental evolution coupled with time-resolved sequencing and phenotyping. We found a doubling of pre-existing variation alone boosts the adaptation by 64.1% and 51.5% in hydroxyurea and rapamycin, respectively. The causative pre-existing and de novo variants were selected on shared targets: *RNR4* in hydroxyurea and *TOR1*, *TOR2* in rapamycin. Interestingly, the pre-existing and de novo TOR variants map to different functional domains and act via distinct mechanisms. The pre-existing TOR variants from two domesticated strains exhibited opposite rapamycin resistance effects, reflecting lineage-specific functional divergence. This study provides a dynamic view on how pre-existing and de novo variants interactively drive adaptation and deepens our understanding of clonally evolving populations.

Key words: **adaptation, drug resistance, pre-existing genetic variation, de novo mutation, budding yeast.**

Introduction

Darwinian evolution promotes phenotypic adaptation in nature and has important implications in biomedical practices. For example, the emergence of drug resistance is the consequence of Darwinian evolution in response to drug selection. According to the classic Neo-Darwinism paradigm, the improvement of population fitness can be achieved by promoting beneficial alleles and purging deleterious alleles. Both pre-existing and de novo variants are subject to this process. One critical question therefore is the relative contribution of pre-existing and de novo variation in driving adaptation to new conditions (Barrett and Schluter 2008; Berg and Coop 2015), which empirically remains poorly characterized (Teotónio et al. 2009; Burke et al. 2014; Vázquez-García et al. 2017; Kosheleva and Desai 2018). Multiple factors can influence the relative contribution, such as the level of pre-existing variation, the variant-specific fitness effect, and the type and duration of selective regimes (Long et al. 2015). Pre-existing variants are predicted to disproportionately drive adaptation when de novo beneficial mutations are rare and have small selection coefficients, or when selection is transient (Hermisson and Pennings 2005). Pre-existing variants can also rapidly respond to stress given their immediate availability and higher resilience to drift (Barrett and Schluter 2008).

Connecting genotypes, phenotypes, and fitness changes in a causally cohesive manner is challenging in both natural and clinical populations, but feasible in experimental populations. Experimental evolution can reveal the molecular determinants of adaptation across a wide range of biological systems with unprecedented resolution (Long et al. 2015). It can be initiated from populations with known levels of pre-existing variation, evolved under fixed selection regimes, and preserved *ad infinitum* as frozen fossil records that can be revived and studied in detail. Experimental evolution of initially isogenic populations has confirmed theoretical predictions such as how expanding clones carrying different beneficial mutations compete with each other (clonal interference), and how neutral or slightly deleterious mutations can hitchhike to higher frequencies together with beneficial mutations

Article

(Gerrish and Lenski 1998; Barrick et al. 2009; Herron and Doebeli 2013; Kvitek and Sherlock 2013; Lang et al. 2013; Levy et al. 2015; Payen et al. 2016; Venkataram et al. 2016). In contrast, it is more challenging to pinpoint the causal relationships in heterogeneous populations due to the large number of segregating variants and the effects of genetic linkage. Previous studies in experimental evolution using heterogeneous populations of budding yeast, fly, and Virginia chicken have all shown that pre-existing variation alone can drive adaptation (Burke et al. 2010; Parts et al. 2011; Burke et al. 2014; Sheng et al. 2015; Kosheleva and Desai 2018). In our recent study, we evolved heterogeneous yeast populations derived from two genetically divergent parents (hereafter referred to as "two-parent population") in cancer drugs and show the joint contributions and interplay of pre-existing and de novo variants to adaptation (Vázquez-García et al. 2017).

To better understand such interplay, two important questions remain to be explored: (1) how the levels of pre-existing variation quantitatively affect the adaptation rate and yield and (2) whether pre-existing and de novo variants act upon shared selection targets and mechanisms. These questions have direct implications on our understanding of the evolution of resistance to chemotherapy and antimicrobials (Turner and Reis-Filho 2012; Palmer and Kishony 2013). To this end, we evolved highly heterogeneous yeast populations derived from four diverged parents (Cubillos et al. 2013) (hereafter referred to as "four-parent population," fig. 1A) under anticancer drugs. We used rapamycin (RM) and hydroxyurea (HU) because of their high specificities and well-studied mechanisms of action. As the target of RM, both *TOR1* and *TOR2* can form the RM-sensitive TOR complex 1 (TORC1) in yeast but only *TOR2* can also form the RM-insensitive TORC2. HU selectively inhibits ribonucleotide diphosphate reductase (*RNR*), preventing cells from leaving the G1/S phase of the cell cycle. The two drugs also cover the action of two common modes of antimicrobial and anticancer drugs: inhibition of nucleic acid synthesis (HU) and inhibition of protein synthesis and cell growth (RM). In comparison to the two-parent population, the four-parent population has approximately doubled the level of pre-existing variation: 1 single nucleotide polymorphism (SNP)/120 bp versus 1 SNP/230 bp (Cubillos et al. 2013). In this experimental system, we define pre-existing variation as the segregating natural variants that accumulated over long evolutionary timescale (i.e., after the diversification of the four parental strains) and define de novo mutations as new variants that arose within much shorter evolutionary timescale (i.e., during either the intercross or the drug selection phase of this experiment). We monitored and dissected the adaptation of the four-parent populations in the two drugs by time-resolved population genome sequencing and comprehensive phenotyping. Combined with paralleled experiments using isogenic populations as well as the two-parent populations (Vázquez-García et al. 2017), our unique experimental system provides the first empirical evidence of how higher level of pre-existing variation quantitatively altering the dynamics of evolution. In stark contrast to the two-parent population experiment where only one pre-existing causative variant was mapped, the experimental evolution using four-parent populations revealed more than 20 quantitative trait loci (QTLs) contributing to drug resistance, underlying a complex genetic trait architecture that drives adaptation in populations with higher levels of genetic variation. Moreover, our nucleotide-resolution mapping further revealed that causative pre-existing and de novo variants converged on shared molecular targets but their underlying molecular mechanisms turned out to be significantly differed.

Results

Evolution of Isogenic and Heterogeneous Populations to RM and HU

We asexually evolved diploid *Saccharomyces cerevisiae* populations with different levels of pre-existing variation for 32 days (>50 generations) under RM, HU, and no drug control conditions (fig. 1A and supplementary tables S1 and S2, Supplementary Material online). The isogenic populations—WA, NA, WE, and SA—corresponding to strains from the West African, North American, Wine/European, and Sake subpopulations, respectively, were homogeneous, corresponding to clonal expansions of the four respective parents. The two-parent populations were heterogeneous, derived from the WA and NA parents by 12 rounds of intercrossing (Parts et al. 2011; Vázquez-García et al. 2017). The four-parent populations derived from all the four parents (Cubillos et al. 2013), thus were highly heterogeneous with doubled segregating variants than their two-parent counterparts. Therefore, the isogenic, two-parent and four-parent populations provide a unique system with increasing levels of pre-existing variation at the onset of selection, which is critical for quantitatively dissecting the impact of pre-existing variation on evolution. We evolved two replicates of each isogenic parental population and eight replicates of the four-parent populations by periodic population bottlenecks of 1/10 every 2 or 3 days and stored a subsample of each transfer to create a dense fossil record (T0 to T14 in HU and T0 to T15 in RM, supplementary table S1, Supplementary Material online). The population size varied between $\sim 10^7$ and 10^8 cells. All the populations are labeled in a format of "population_condition_replicate_time" (e.g., "NA_HU_1_T2" represents the NA population evolved in HU, the first replicate at T2).

To track the evolutionary dynamics comprehensively, we revived the frozen subsamples of all the populations across all the time points (supplementary tables S1 and S2, Supplementary Material online). We estimated their fitness-related properties by spotting assay and precise measurements of their doubling time (fig. 1B and supplementary figs. S1–S3, Supplementary Material online). In the RM experiment, the overall adaptive gain of the four-parent and two-parent populations throughout the whole experiment was similar (45.3% vs. 42.6% of doubling time reduction, Mann–Whitney *U* test, $P = 0.96$). However, the early-phase adaptive gain (T0 to T2) was larger in the four-parent populations (19.2% vs. 11.2% of doubling time reduction, Mann–

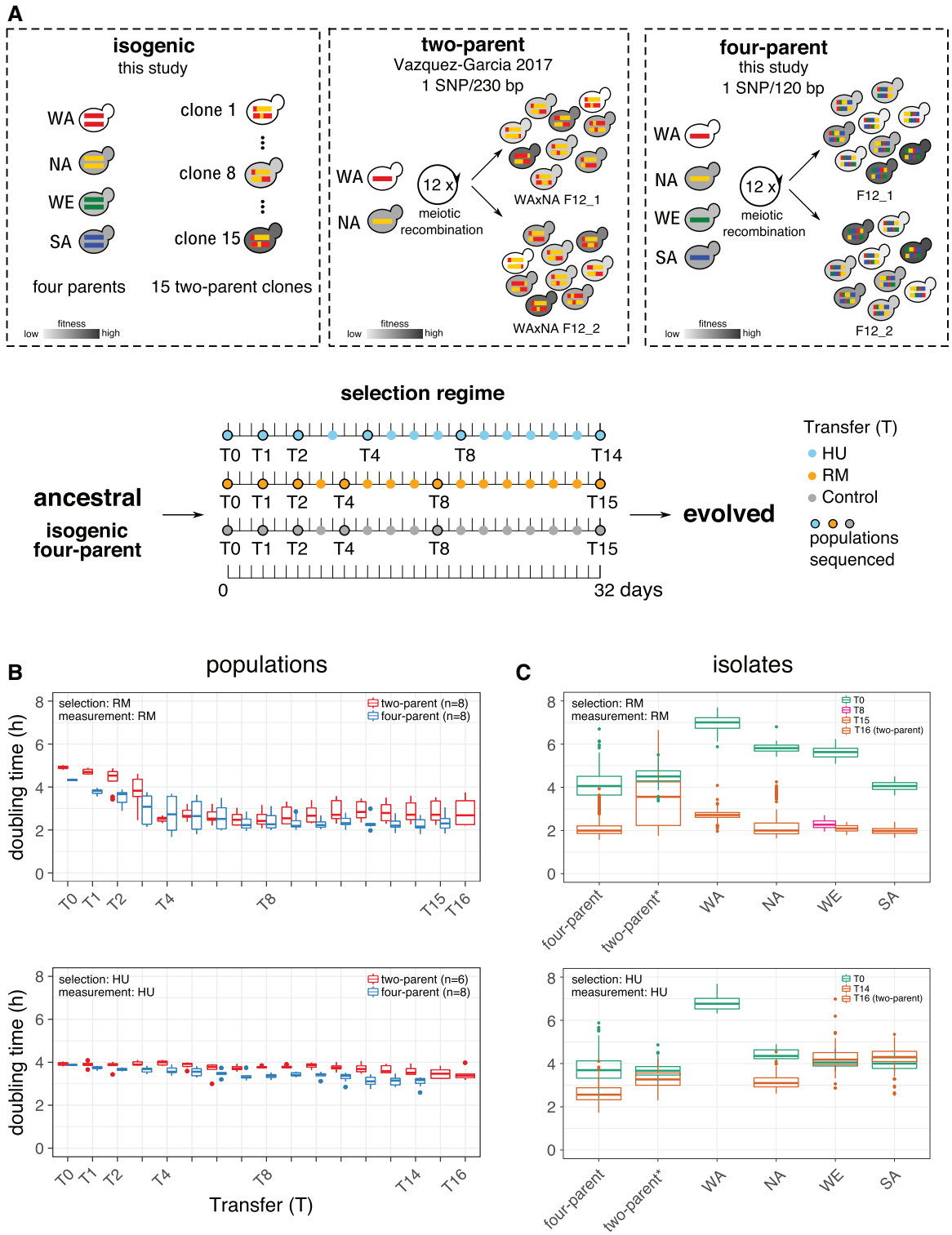

Fig. 1. Evolution of isogenic and heterogeneous populations to RM and HU. (*A*) Ancestral populations with increasing pre-existing variation from isogenic, two-parent to four-parent populations (top) and timeline of selection experiment for isogenic and four-parent populations (bottom). The timeline of two-parent selection experiment is listed in supplementary table S1, Supplementary Material online. Random subsamples of the initial populations, and of the first, second, fourth, eighth, and the last transfer (T14 for HU and T15 for RM in the isogenic and four-parent populations; T16 for HU and RM in the two-parent populations) were sequenced in bulk. The experimental evolution of 15 two-parent clones was performed only in HU condition. (*B*) Doubling time in RM (top) and HU (bottom) of the randomly sampled bulk populations after each expansion cycle. Boxplot shows the doubling time of all the populations during the experimental evolution (biological replicates are indicated in parentheses). (*C*) Doubling time of clonal populations expanded from random, single individuals drawn from the ancestral and endpoint populations (supplementary table S2, Supplementary Material online) in RM (top) and HU (bottom). For each drug, we phenotyped 384 random individuals from both the ancestral and endpoint four-parent populations, as well as 48 and 96 random individuals from each ancestral and endpoint isogenic

Whitney U test, $P = 0.038$), highlighting the advantage of higher level of pre-existing variation in driving rapid adaptation. There was no substantial late stage adaptation (i.e., during the last three time points) in either four-parent or two-parent populations (5.1% of doubling time increase and 1.1% decrease, respectively), suggesting the exhaustion of adaptive potentials within the experimental timescale. In the HU experiment, the adaptation was slow, gradual, and persisted to the end in both the four-parent and two-parent populations, although seemingly greater adaptive gains were observed in the four-parent populations (20.4% vs. 12.3% of doubling time reduction, Mann–Whitney U test, $P = 0.06$). Therefore, a doubling of segregating diversity in the four-parent populations translated into more rapid and likely greater adaptive gains in both RM and HU. No observable adaptation to control condition (no drug) was observed (supplementary fig. S1, Supplementary Material online).

To measure the adaptive gains of individuals independently of their background populations, we randomly isolated >2,600 clones from both ancestral and endpoint populations (supplementary table S2, Supplementary Material online) and measured their respective doubling time. Before selection (T0), the variation in doubling time of the four-parent individuals was much greater than those of the two-parent populations (fig. 1C, coefficient of variation = 0.16 vs. 0.08 in both RM and HU). Thus, the higher genetic diversity of the four-parent populations also translated into higher variation in the key fitness component under selection, creating a necessary foundation for faster adaptation. The mean adaptive gain of the four-parent individuals at the endpoint exceeded that of their counterparts from the two-parent populations, with a doubling time reduction of 48.2% versus 27.2% in RM (Mann–Whitney U test, $P < 2.2 \times 10^{-16}$) and 29.9% versus 11.2% in HU (Mann–Whitney U test, $P < 2.2 \times 10^{-16}$). These measurements further verified the accelerated adaptation in populations with higher level of pre-existing variation (fig. 1C and supplementary fig. S4, Supplementary Material online).

Interestingly, the isogenic parental populations exhibited distinct evolutionary dynamics in RM and HU conditions. In RM, all the isogenic lines grew faster than their ancestral populations regardless of the founding genetic backgrounds (fig. 1C and supplementary figs. S1, S3, and S4, Supplementary Material online, Mann–Whitney U test, $P < 2.2 \times 10^{-16}$). Individuals drawn from the NA, SA, and WE endpoint populations reached the same level of adaptation as those from the evolved four-parent populations, whereas those from the WA populations adapted more slowly, which was consistent with their weaker initial growth. In HU, however, only NA managed to adapt (28.2% of doubling time reduction, Mann–Whitney U test, $P < 2.2 \times 10^{-16}$), although still failed to reach the same adaptation level of the four-parent individuals (fig. 1C; mean endpoint doubling time 3.16 vs. 2.62 h, Mann–Whitney U test, $P < 2.2 \times 10^{-16}$). SA and WE grew worse at the end of HU selection than their respective ancestral states (6.5% of doubling time increase in SA, Mann–Whitney U test, $P = 4.1 \times 10^{-6}$; and 4.2% of doubling time increase in WE, $P = 6.6 \times 10^{-3}$). The WA populations went extinct at earlier time points (T2).

In summary, we found a general trend of positive correlations between the levels of pre-existing variation and the rate of adaptation, the absolute adaptive gains, and the endpoint performance regardless of the selection regimes. These observations collectively suggest a greater adaption potential for populations with higher genetic diversity, likely enabled by a richer reservoir of selection targets that are immediately accessible.

De novo Mutations Are Prevalent for RM Resistance but Background-Dependent for HU in Isogenic Populations

We first profiled de novo mutations in isogenic parental populations (supplementary tables S1–S3, Supplementary Material online), which served as a baseline for the comparison with the four-parent populations. In RM, we detected recurrent mutations in *TOR1* and *FPR1* (fig. 2A). Six *TOR1* mutations hit three amino acid sites in all the eight parental populations, indicating *TOR1* as a background-independent selection target for RM resistance. In contrast, the *FPR1* mutations (frame shift and start codon disruption at two amino acid sites) emerged only in the two NA populations. Surprisingly, all the NA clones carrying *FPR1* mutations became haploids during selection. This may be a collective consequence of NA diploids being highly prone to sporulation even in rich medium (Cubillos et al. 2009) and the fact that the loss-of-function *FPR1* mutations are fully recessive and thus favor the haploid status during rapid adaptation (Vázquez-García et al. 2017). The frequency increase of the *TOR1* and *FPR1* mutations agrees well with the doubling time reduction of the populations in which they emerged (fig. 2A), indicating that they are true drivers of the adaptation, rather than hitchhikers or drifters, and that the adaptation is genetic, rather than initially epigenetic and later genetically assimilated (Gjuvsland et al. 2016). Interestingly, there is a slight delay between the mutation frequency increase and the doubling time decrease at T2 and T4 in a few populations. We further phenotyped 192 clones from the relevant populations

Fig. 1. Continued

parental population. The mean doubling time of these individuals were pooled based on their category (e.g., four-parent, two-parent) and time points (e.g., T0, T15) and shown by the boxplots. The details of technical replicates and standard deviation are listed in supplementary table S12, Supplementary Material online. The WA isogenic populations went extinct after T2 in HU. One WE isogenic population in RM was contaminated at T15 and therefore T8 was analyzed instead. *The wide doubling time distribution of two-parent individuals in RM at T16 is due to the coexistence of fast and slow growth individuals with and without driver mutations, see Vázquez-García et al. (2017). Boxplot: center lines = median; boxes = interquartile range (IQR); whiskers = 1.5×IQR; points = outliers beyond 1.5×IQR.

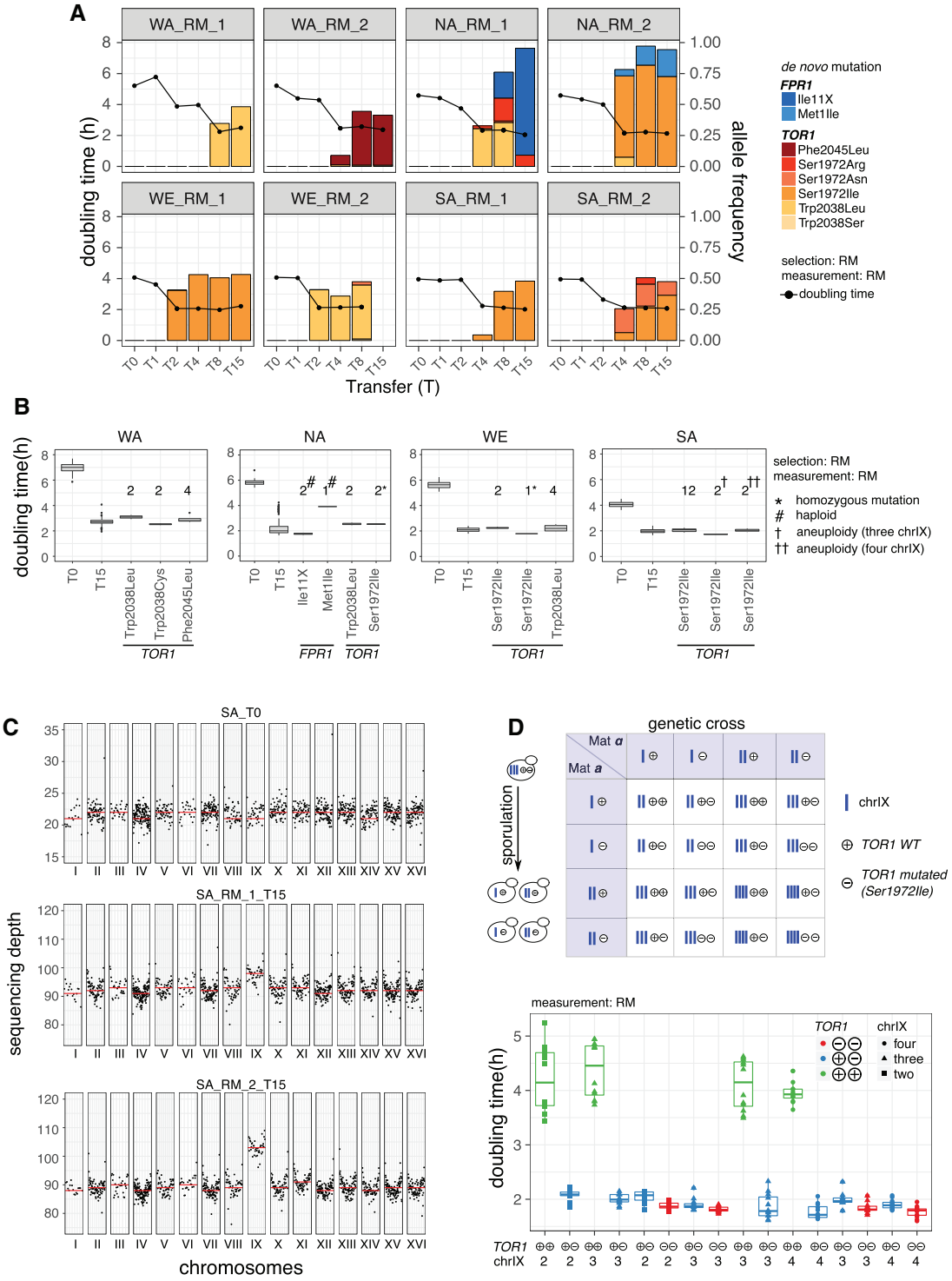

Fig. 2. De novo mutations in *TOR1* and *FPR1* drive RM adaptation in isogenic populations. (*A*) Lines indicate mean doubling time of the bulk population (left *y*-axis). Bars represent frequency dynamics of de novo driver mutations (right *y*-axis). Bar colors indicate different driver mutations in *FPR1* (light-dark blue) and *TOR1* (yellow-brown). (*B*) Doubling time of random individuals drawn from the ancestral (T0, 48 individuals for each parent), RM evolved (T15, 192 individuals for each parent) populations and genotyped individuals. We divided genotyped individuals into groups based on their driver mutations; no individual carried more than one driver mutation. The number above the boxplot indicates the number of genotyped individuals with confirmed driver mutations by Sanger sequencing. (*C*) The genome-wide sequencing depth of SA population at T0 and two replicates at T15 evolved in RM, measured by bulk population sequencing. Genomic positions are shown on the *x*-axis and sequencing depth on the *y*-axis. Each point indicates the mean sequencing depth of a 10-kb window and the red line indicates median sequencing depth of each chromosome. (*D*) Design (top) and doubling time (bottom) of a genetic cross experiment. We crossed haploid derived from spores obtained from individuals drawn from the RM evolved (T15) SA populations to generate diploids with known configurations of driver mutation genotypes and chromosome IX copy number. "+" and "−" = *TOR1* genotypes, WT and de novo mutated respectively. Blue bar = chromosome IX. Marker shape = chromosome IX copy number, marker color = *TOR1* genotype. Of note, there are two distinct clusters of doubling times for the *TOR1* WT strains,

and observed none or few resistant clones at T2 but more at T4 (supplementary fig. S5G, Supplementary Material online), which is consistent with the doubling time measurements (fig. 2A) as well as the population level spotting assay (supplementary fig. S1, Supplementary Material online). Such slight delay therefore can be explained by either early and low-frequency mutations that escaped our detection or clone frequencies increasing during the phenotyping phase.

To quantify the individual contributions of the *TOR1* and *FPR1* mutations to RM adaptation, we isolated and estimated the doubling time of individual clones carrying these mutations (fig. 2B and supplementary table S4, Supplementary Material online). Except for the *FPR1* Met1Ile mutation, the doubling time reduction conferred by each individual mutation equals (e.g., *TOR1* S1972I in WE) or approaches (>90%, e.g., *TOR1* W2038L and S1972I in NA) that of the evolved population carrying these mutations (fig. 2B), therefore capable of explaining almost the complete adaptive gains. All RM-adapted populations showed comparable growth performance in the presence or absence of RM, suggesting that the RM adaptation had plateaued within the experimental timescale (supplementary fig. S4, Supplementary Material online). The *TOR1* mutations recurrently emerged in different genetic backgrounds (Ser1972Ile in NA, SA, and WE and Trp2038Leu in WA and WE) and conferred complete tolerance to RM (fig. 2B). In the NA background, a larger adaptive gain was acquired by the *FPR1* Ile11X frame shift mutation than by the *FPR1* start codon disruption (Met1Ile) (69.8% vs. 32.9% of doubling time reduction, Mann–Whitney *U* test, $P = 2.7 \times 10^{-6}$, fig. 2B), which agreed with the near fixation of *FPR1* Ile11X in NA_RM_1 and the lower frequency of the *FPR1* Met1Ile in NA_RM_2 (fig. 2A). Given that both mutations should lead to complete loss-of-function, this distinction is intriguing. In the WE background, the *TOR1* Ser1972Ile homozygous clones grow faster than those with the heterozygous mutation (fig. 2B, 68.1% vs. 59.8% of doubling time reduction, Mann–Whitney *U* test, $P = 1.9 \times 10^{-4}$), giving them a competitive edge. One would expect continued selection to drive the homozygote state to fixation via loss of heterozygosity (LOH), as demonstrated in our previous study (Vázquez-García et al. 2017).

Population-wide whole-genome sequencing revealed the copy number gain of chromosome IX (chrIX) under RM selection in both replicates of the SA populations (fig. 2C and supplementary table S3, Supplementary Material online). Quantitative PCR (qPCR) further confirmed that the RM-evolved diploid SA clones carried three or four copies of chrIX (supplementary notes, Supplementary Material online). We noticed a strong association between chrIX copy number and heat sensitivity in the SA background, based on which we estimated ~12.5% and ~8.3% of the evolved population (SA_RM_2_T15) carried three and four copies of chrIX, respectively (supplementary fig. S5F, Supplementary Material online), consistent with our estimates based on sequencing depth (fig. 2C). All the chrIX-gained SA clones also carried the *TOR1* Ser1972Ile heterozygous mutation, and we found those with three copies of chrIX grew faster in RM than those with two or four copies (Mann–Whitney *U* test, $P = 6.90 \times 10^{-5}$ and $P = 3.43 \times 10^{-3}$, respectively) (fig. 2B). To dissect the interactions between the *TOR1* Ser1972Ile mutation and chrIX aneuploidy, we constructed a genetic cross of strains with all possible combinations of *TOR1* (wild type or mutated) and chrIX copy number (2, 3, and 4 copies) and measured their respective doubling time (fig. 2D, supplementary notes). We found the *TOR1* Ser1972Ile mutation as a major contributor to the RM resistance (53.2% and 56.1% of doubling time reduction for heterozygous and homozygous mutation, respectively) whereas the copy number gain of chrIX only conferred marginal benefits.

In sharp contrast to RM selection, isogenic parental populations propagated in HU almost uniformly failed to acquire de novo mutations except for the *RNR4* mutations (Arg34Ile and Lys114Met) in the NA populations. To confirm that such contrast was not due to the limited number of replicates, we performed a second batch of experimental evolution in HU. In this batch, we evolved three replicates for each parent, phenotyped the populations by spotting assay and genotyped *RNR2* and *RNR4* (supplementary fig. S1 and tables S2 and S4, Supplementary Material online). Again, the NA populations showed clear fitness improvement associated with *RNR2* and *RNR4* mutations. Among the three WE and three SA populations in HU, only one SA population acquired a beneficial *RNR4* mutation, whereas all the others showed limited fitness gain (supplementary fig. S1G, Supplementary Material online). All the WA populations died out early on. These results are consistent with those of the first batch of experimental evolution. Therefore, we concluded that different homozygous genetic backgrounds had important effects on the acquisition of de novo mutations in HU. To further dissect the background-dependent constraints, we evolved 15 clones (each with three replicates) randomly drawn from the two-parent population (WA x NA F12) in HU. These clones should all harbor a mosaic of comparable numbers of NA (highly adaptable) and WA (poorly adaptable) alleles. After 32-day evolution, all the 45 populations adapted to HU, regardless of their initial tolerance to HU (supplementary fig. S1, Supplementary Material online). All evolved populations acquired beneficial de novo mutations in at least one of *RNR2* and *RNR4*. The amino acid sites 169 (Y169H) and 280 (A280V) of *RNR2* as well as 34 (R34I) and 111 (P111H) of *RNR4* appeared to be driver mutation hotspots (supplementary tables S2 and S4, Supplementary Material online). Also, clones carrying WA *RNR2* and *RNR4* alleles could acquire the beneficial *RNR2* and *RNR4* de novo mutations, showing that

FIG. 2. Continued
which is due to the batch effect of two different scanners used to monitor the colony growth (e.g., local variation in humidity within the cabinet). Nevertheless, this did not influence the conclusion that *TOR1* was the driver mutation rather than the chrIX copy number changes. Boxplot: center lines, median; boxes, interquartile range (IQR); whiskers, 1.5×IQR. Data points beyond the whiskers are outliers.

the incapacity of isogenic WA populations to adapt should come from the epistatic constraints of the original WA background. Taken together, the evolutionary dynamics in HU is strongly background dependent.

De novo Mutations in *TOR1*, *TOR2*, and *FPR1* Drive RM Adaptation in Heterogeneous Populations

Both pre-existing and de novo variants could contribute to adaptation in the four-parent populations. Theoretically, the frequency spectrum of pre-existing parental alleles should center on 0.25 in these populations. At T0, we found a median allele frequency of 0.21 (WA), 0.26 (NA), 0.26 (WE), and 0.26 (SA) for the four parental backgrounds (Cubillos et al. 2013). In contrast, the initial frequencies of de novo mutations (acquired during the crossing or selection phases) are expected to be extremely low (Vázquez-García et al. 2017). We found recurrent de novo driver mutations in *FPR1*, *TOR1*, and *TOR2* (fig. 3*A*). Among them, we noticed that the *FPR1* mutations occurred in all the replicates derived from one intercrossed population, whereas the *TOR1* mutations were found in all the replicates derived from the other. We reasoned that these drivers should have emerged during the shared crossing phase and then expanded independently during the selection phase. As an evidence for this, we found similar frequency patterns of haplotype blocks in the replicates derived from the same intercrossed population, reflecting an expansion of the same clones present at T0 (supplementary fig. S6, Supplementary Material online). We found recurrent *TOR1* mutations at the same amino acid site as the isogenic populations, suggesting that these are the primary RM selection targets regardless of the genetic backgrounds. In one population (F12_2_RM_4), we found a *TOR2* Ser1975Ile mutation (fig. 3*A*) located in the RM-binding domain and being paralogous to *TOR1* Ser1972, implying conserved RM selection targets between *TOR1* and *TOR2* (Helliwell et al. 1994). The clones containing this *TOR2* mutation revealed a mixture of heterozygous and homozygous loci, which explained its >0.5 frequency in the population. The doubling time of *TOR2* homozygous mutants in RM is significantly shorter than that of the heterozygous clones (mean: 1.77 vs. 2.18 h, Mann–Whitney *U* test, $P = 3.9 \times 10^{-4}$). The doubling time of all the clones carrying driver mutations (1.83–2.34 h) were substantially shorter than that of clones without these drivers (3.45 h) drawn from the adapted populations (fig. 3*B*), suggesting clear phenotypic contributions from these de novo driver mutations.

In contrast to RM, we did not detect any de novo driver mutations in the four-parent populations evolved under HU although it is possible that short-read sequencing could not accurately capture de novo structural rearrangements in populations. Nevertheless, given the obvious phenotypic adaptation to HU (fig. 1*B* and *C* and supplementary fig. S4, Supplementary Material online), and the substantial parental allele frequency changes across the genome at later time points (supplementary fig. S7, Supplementary Material online), we conjectured that pre-existing variants have dominantly driven the HU adaptation in four-parent populations.

Pre-existing Variation Provides Multiple Selection Targets to Drive Adaptation in Heterogeneous Populations

We next investigated how the pre-existing variation in the four-parent populations contributed to the RM and HU adaptation. We searched for genomic regions (i.e., QTLs) with steady allele frequency changes across multiple time points and replicates. At later time points (T4 to T15), we observed strong allele frequency shifts over large genomic regions, reflecting haplotype blocks of drug-resistant clones rising to high frequencies in both selection regimes (supplementary figs. S6 and S7, Supplementary Material online). Therefore, we measured allele frequency changes before the clone emergence (T0-T4 for HU and T0-T2 for RM) to map QTLs with different stringency cut-offs (i.e., 99% and 95% quantiles; see Materials and Methods).

In HU, two QTLs passed the 99% quantile cut-off and seven more passed the 95% cut-off (fig. 4*A* and supplementary table S5, Supplementary Material online) with a median size of 22 kb and containing ten genes on average. The peak of the strongest QTL (chrVII: 841–863 kb) hits the *RNR4* gene. The $RNR4^{WE}$ allele was selected over the other three parental alleles throughout our experiment (fig. 4*B* and *C*). We validated the selective advantage of the $RNR4^{WE}$ allele by a growth-based reciprocal hemizygosity assay (Warringer et al. 2017). The diploids carrying a weak $RNR4^{NA}$ allele grew 15.7% slower than the otherwise identical diploids carrying the strong $RNR4^{WE}$ allele (normalized by their growth in the control medium, Mann–Whitney *U* test, $P = 3.21 \times 10^{-3}$, fig. 4*D* and supplementary fig. S5*A*, Supplementary Material online). The other strong QTL (chrIV: 503–563 kb) encompasses the highly pleiotropic *ENA1*, *ENA2*, and *ENA5* transporter gene cluster (Warringer et al. 2011) with the SA allele driving toward fixation in all replicates (supplementary fig. S8, Supplementary Material online). Four of the seven QTLs passing the 95% quantile exhibited continuous and directional allele frequency changes until the end of the experiment (supplementary table S6 and fig. S8, Supplementary Material online), whereas the allele frequency changes of the other three QTLs wore off earlier. Given that there were no detectable de novo driver mutations, the latter was probably due to overwhelmed competition from clones carrying the beneficial versions of strong QTLs (e.g., $RNR4^{WE}$, ENA^{SA}).

Similarly, we identified four QTLs passing the 99% quantile cut-off in RM (supplementary table S5 and fig. S9, Supplementary Material online). The two strongest QTLs cover the *TOR1* and *TOR2* genes, respectively. Interestingly, the WE and SA alleles of *TOR1* and *TOR2* show opposite allele frequency changes: $TOR1^{SA}$ and $TOR2^{WE}$ were selected for, whereas $TOR1^{WE}$ and $TOR2^{SA}$ were selected against (fig. 5*A*). We validated such parental-specific allelic variation by reciprocal hemizygosity (fig. 5*B* and supplementary fig. S5, Supplementary Material online). After normalizing for growth in the control medium, clones carrying the strong $TOR1^{SA}$ allele grew faster and reached a higher yield than those with the weak $TOR1^{WE}$ allele in RM (Mann–Whitney *U* test, $P = 3.1 \times 10^{-4}$ and $P = 1.8 \times 10^{-3}$, respectively). Clones carrying the strong $TOR2^{WE}$ allele showed significantly higher

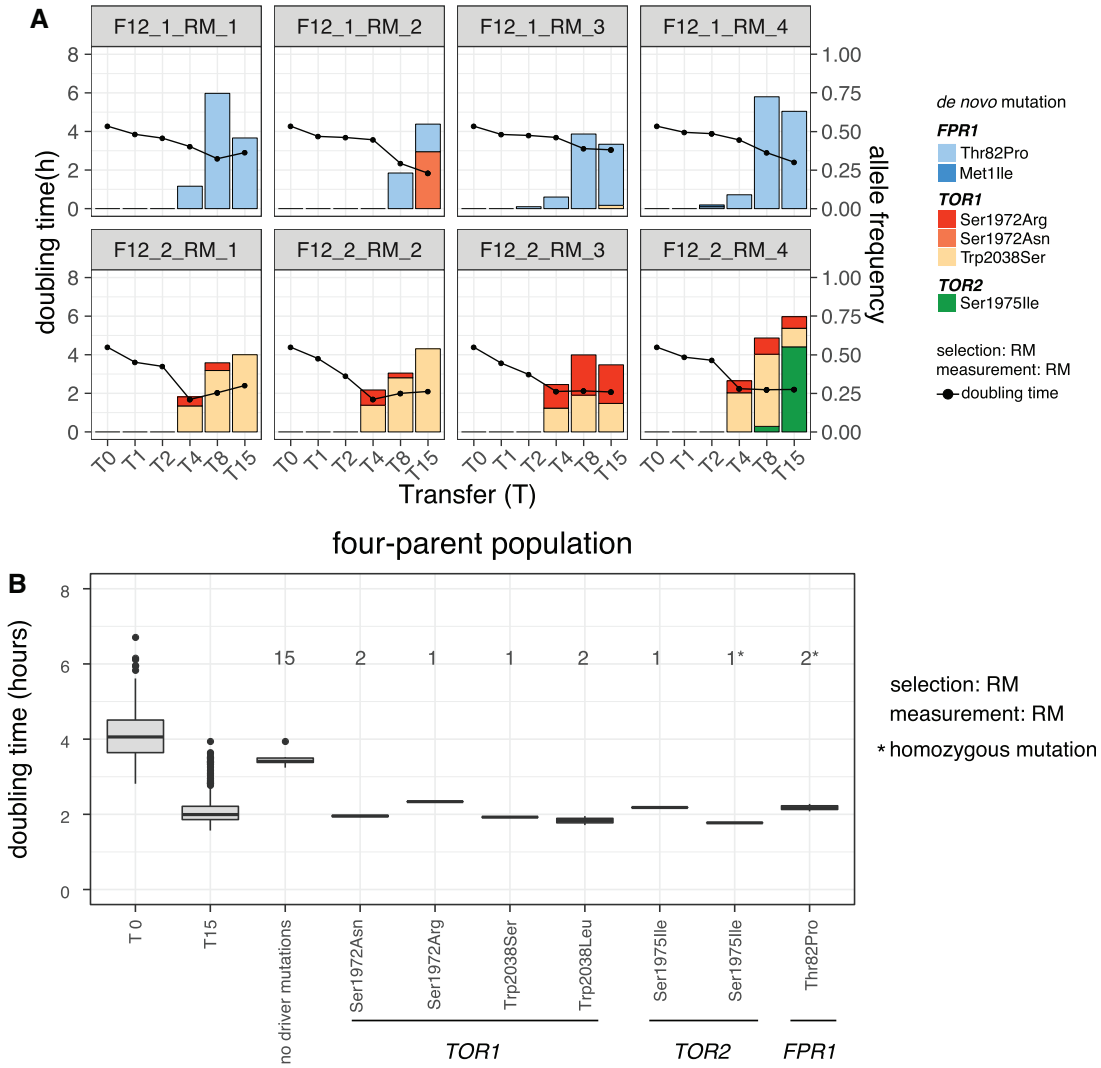

FIG. 3. De novo mutations in *TOR1*, *TOR2*, and *FPR1* drive RM adaptation in heterogeneous populations. (*A*) Lines indicate mean doubling time of the bulk population (left *y*-axis). Bars represent frequency dynamics of de novo driver mutations emerging in four-parent populations adapting to RM (right *y*-axis). Bar colors indicate different driver mutations in *FPR1* (light-dark blue), *TOR1* (yellow-red), and *TOR2* (green). Top and bottom panels show replicates from F12_1 and F12_2, respectively. (*B*) Doubling time of random individuals drawn from the ancestral (T0, 384 individuals) and RM evolved (T15, 384 individuals) populations. We divided genotyped individuals into groups based on their driver mutations; no individual carried more than one driver mutation. The number above each boxplot indicates the number of genotyped individuals by Sanger sequencing. Boxplot: center lines, median; boxes, interquartile range (IQR); whiskers, 1.5×IQR. Data points beyond the whiskers are outliers.

yield (Mann–Whitney *U* test, $P = 1.5 \times 10^{-4}$). Nine additional QTLs passed the 95% quantile cut-off. We considered *SNQ2*, *NPR3*, *KOG1*, and *CTF8* to be strong candidates for driver QTLs. Among them, *CTF8* has been experimentally validated to confer RM resistance in the two-parent populations (Vázquez-García et al. 2017). *SNQ2* encodes a multidrug resistance ABC transporter. *NPR3* and *KOG1* act together with TOR in nutrient signaling pathway. Several other QTLs locate in subtelomeric regions, with the one at the right arm of the chromosome XI (chrXI-R) containing the multidrug resistance-associated genes *YKR103W* and *YKR104W* (Mason et al. 2003). Based on the end-to-end genome assemblies of the four parental strains (Yue et al. 2017), these two subtelomeric genes were found to be absent in the WE subtelomere, potentially explaining its dramatic allele frequency decrease during RM selection. The strong RM QTLs such as *TOR1*, *TOR2*, *NPR3*, *CTF8*, and *SNQ2* persisted until late time point (supplementary tables S5 and S6 and fig. S8, Supplementary Material online), despite the emergence of driver-mutation-carrying clones. We found the four parental backgrounds equally likely to donate the fitter or less fit alleles to the four-parent populations. For example, at two of the four strongest RM QTLs (supplementary table S5, Supplementary Material online), the SA allele was the most unfit with substantial allele frequency decreases, despite the SA background being the fittest based on the isogenic parental populations (fig. 1C). Similarly, two strong RM QTLs showed the WA allele as the fittest, despite the WA background being the most unfit in the isogenic parental populations. The inheritance of drug resistant variants from all the founder populations provides support to how higher level of genetic variation translates into higher rate of adaptation.

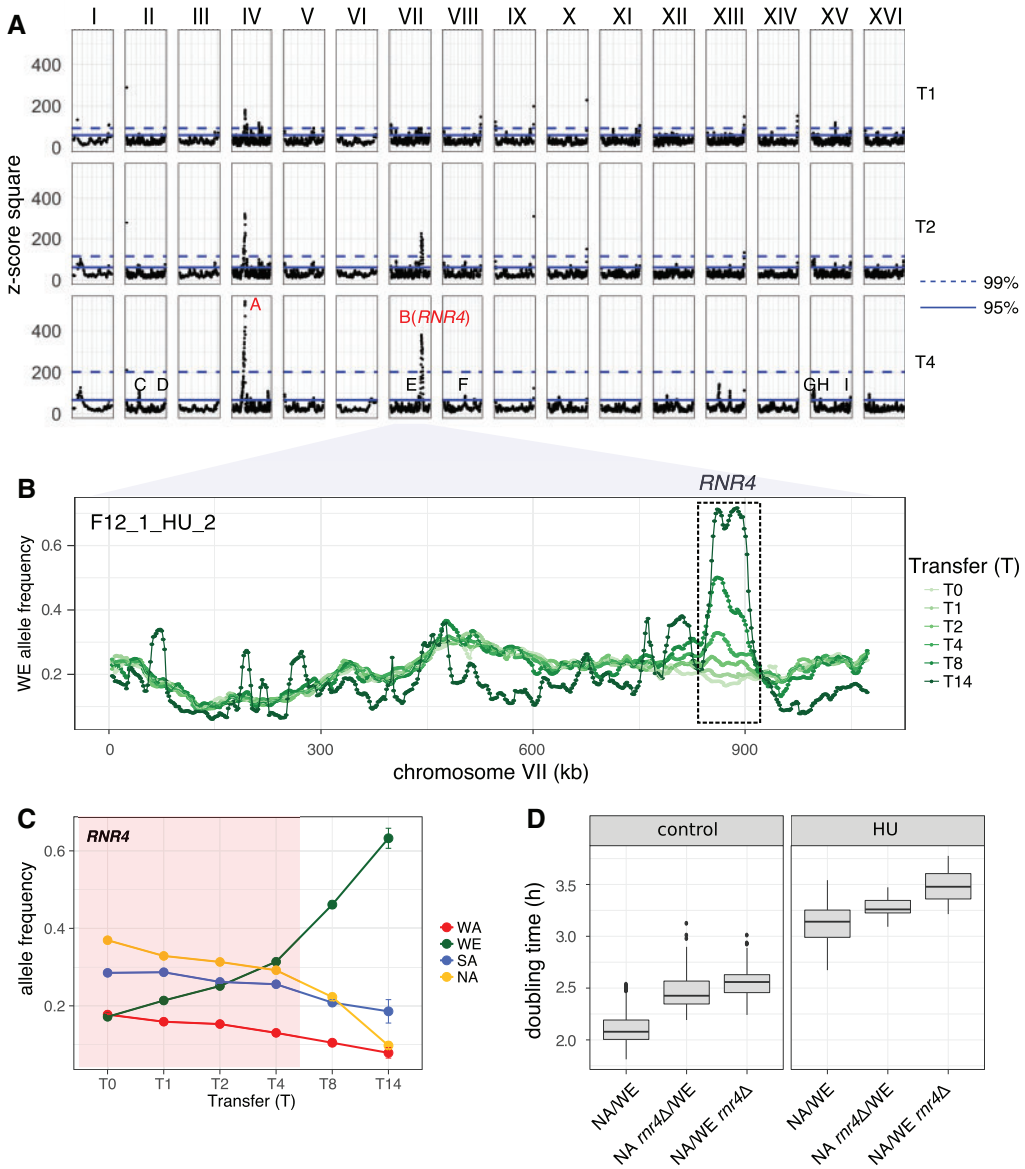

Fig. 4. *RNR4* QTL drive adaptation in the four-parent populations in HU. (*A*) The *z*-score square underlies QTLs and is derived from allele frequency changes from T0 to early phase of selection (T1–T4). Dashed and solid lines indicate 99% and 95% quantile cut-off, respectively. Strong QTLs are labeled in red and weak ones are in black (coordinates listed in supplementary table S5, Supplementary Material online). We filtered out QTLs that mapped to repetitive regions as well as those detected in YPD control condition (supplementary fig. S9, Supplementary Material online). (*B*) WE allele frequency changes in chromosome VII in F12_1_HU_2 four-parent population evolved in HU from T0 to T14. The region in the black box contains the *RNR4* QTL. (*C*) Frequency changes (mean) of the four *RNR4* alleles from T0 to T14, showing 1:3 segregating pattern (one strong allele vs. three weak alleles). The error bars indicate the standard deviation of the eight replicates. The region highlighted in red indicates the early phase of selection used for QTL mapping. (*D*) Doubling time of *RNR4* reciprocal hemizygotes measured in HU and control experimentally confirmed the *RNR4* causative variants. Boxplot: Center lines, median; boxes, interquartile range (IQR); whiskers, 1.5×IQR. Data points beyond the whiskers are outliers.

Shared Selection Targets between Pre-existing and de novo Variants Act via Distinct Mechanisms

The recurrent de novo mutations and QTLs identified in the same genes (*RNR4* in HU and *TOR1*, *TOR2* in RM) showed a pattern of selection on shared molecular targets over both short and long evolutionary timescales. To our knowledge, this is the very first direct evidence of pre-existing and de novo variants being simultaneously revealed upon convergent targets in any evolutionary experiments (Long et al. 2015). To understand this pattern in-depth, we compared the pre-existing and de novo variants identified in isogenic, two-parent and four-parent populations (supplementary table S7, Supplementary Material online, fig. 6). The HU-resistant $RNR4^{WE}$ allele has a single derived amino acid change (Ala161Thr) located within the ribonucleotide reductase domain, which is predicted to be functionally important based on sequence analysis (see Supplementary notes). The *RNR4* de novo driver mutations locate in the same domain but at

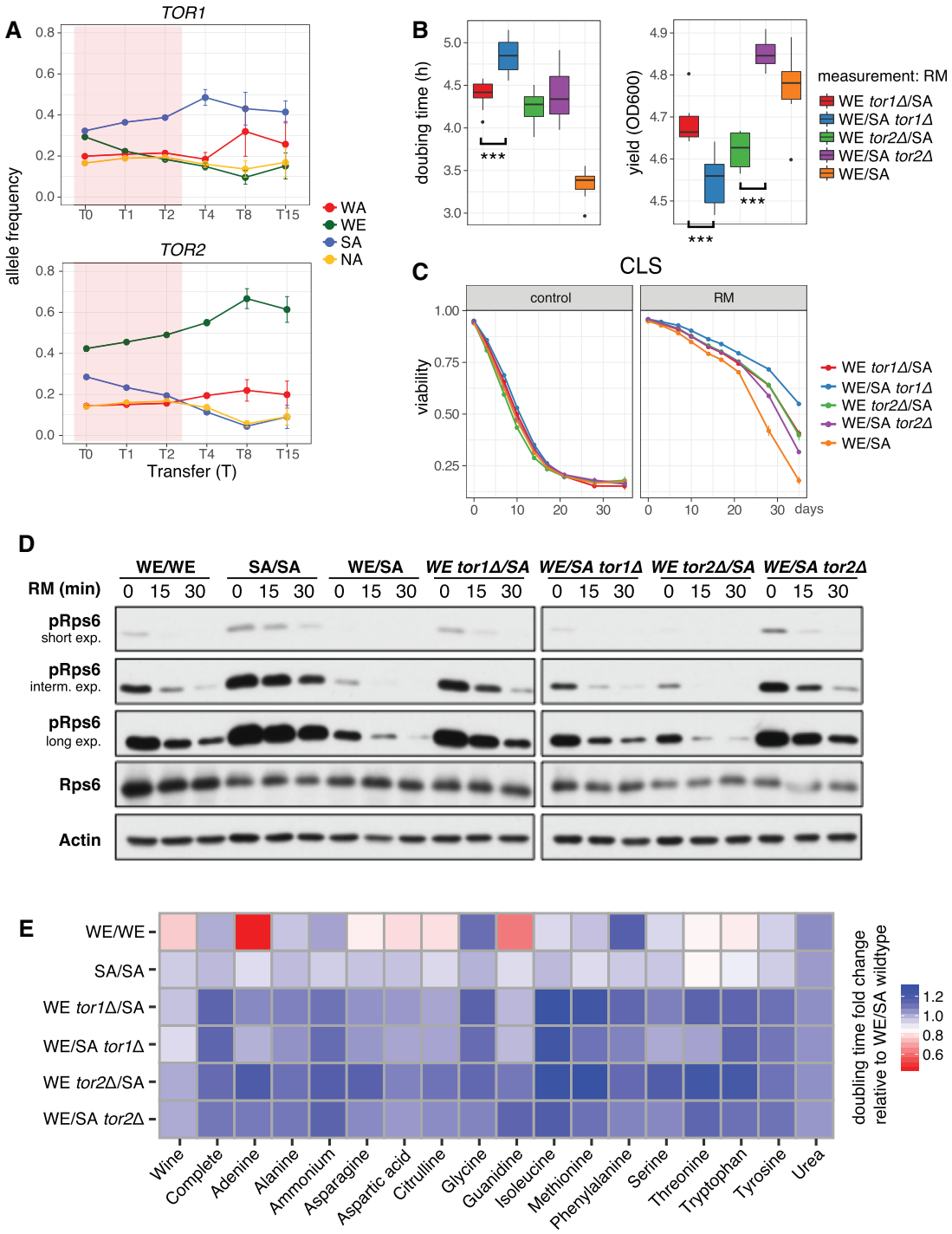

Fig. 5. *TOR1* and *TOR2* allelic variation. (*A*) *TOR1* (top) and *TOR2* (bottom) allele frequency changes of the four-parent populations during RM selection. The region highlighted in red indicates the early phase of selection used for QTL mapping. The points and error bars indicate the mean and standard deviation of all the eight replicates. (*B*) Doubling time (left) and yield (right) of WE/SA hybrid with *TOR1* and *TOR2* reciprocal hemizygote deletions confirm the causative variants for RM resistance. The doubling time and yield were extracted from the growth curve measured in YPD with RM by Tecan plate reader. (*C*) CLS of *TOR1* and *TOR2* reciprocal hemizygotes (WE/SA) in the presence and absence of RM. (*D*) Characterization of the TORC1 activity by immunoblot of Rps6 phosphorylation in WT parents, hybrid and *TOR1*, *TOR2* reciprocal hemizygotes. Cells were treated with RM (200 ng/ml) for the time indicated (minute). Total lysates were resolved by SDS-PAGE on 10% polyacrylamide gels and analyzed by immunoblot. Actin was used as loading control. The "short," "interm.," and "long" panels indicate the exposure time of the membrane to the film. (*E*) Growth phenotypes of wild type strains and *TOR1*, *TOR2* reciprocal hemizygotes in 18 environments, corresponding to synthetic wine must and single nitrogen source environments at nitrogen limiting concentrations. Heat map shows the fold change in doubling time compared with WE/SA wild type hybrid.

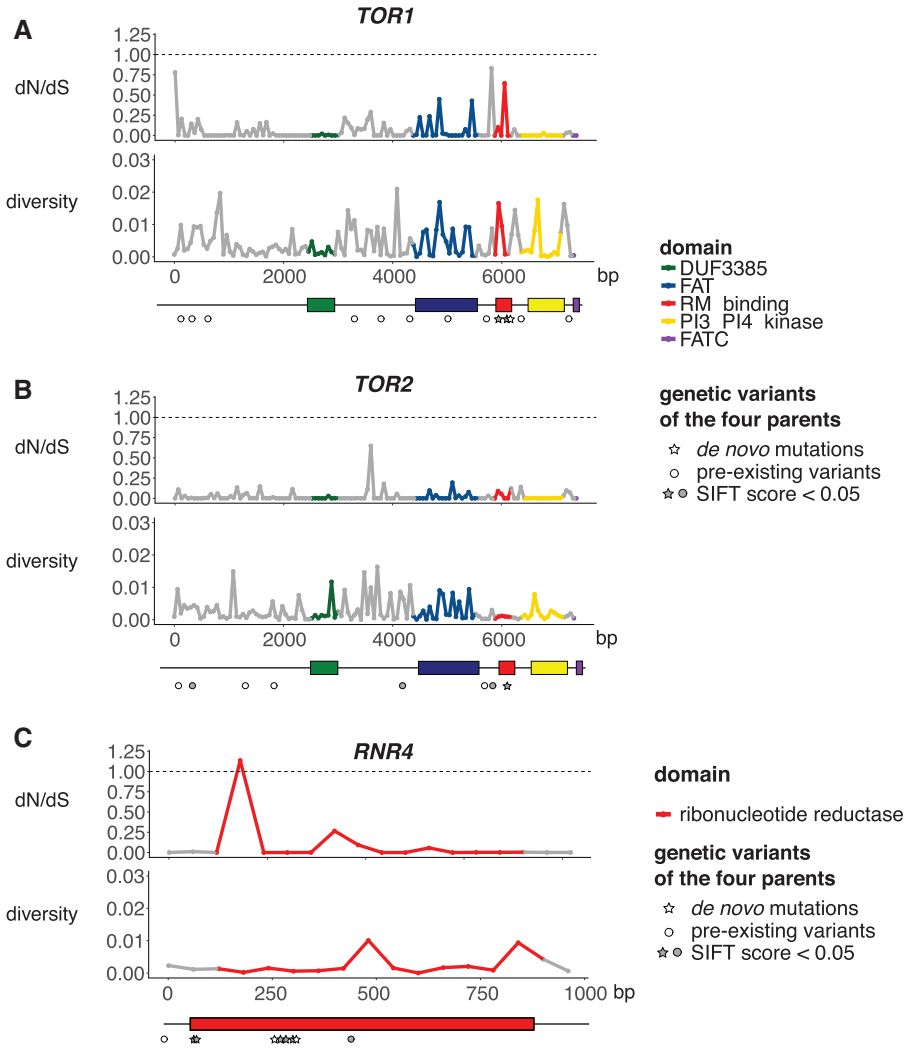

Fig. 6. Sequence analysis of *TOR1*, *TOR2*, and *RNR4*. The ratio of nonsynonymous and synonymous substitutions (dN/dS) and sequence diversity analysis of (*A*) *TOR1*, (*B*) *TOR2*, and (*C*) *RNR4*. All the plots are based on 60-bp window for each gene. The dN/dS and diversity value was calculated using the sequences from the 1002 Yeast Genomes project. Functional domains are highlighted with different colors. The dashed line shows dN/dS = 1, indicating no selection (neutral). Values above 1 indicate positive selection and below 1 indicate purifying or stabilizing selection. Circle indicates the positions of pre-existing variants of the four parental strains. Star indicates de novo mutations identified in the experimental evolution of the isogenic, two-parent and four-parent populations (supplementary table S7, Supplementary Material online). Gray color represents variants with significant SIFT score, indicating positions of high conservation.

different sites (supplementary table S7, Supplementary Material online). All the de novo mutations in the *TOR1*, *TOR2* paralogs hit the highly conserved RM-binding domain, where they prevent the binding of the FKBP12-RM complex and thereby confer RM resistance (Heitman et al. 1991; Cafferkey et al. 1993; Helliwell et al. 1994; Stan et al. 1994; Loewith and Hall 2011). In contrast, none of the *TOR1* and *TOR2* pre-existing variants occur in this domain and almost all locate outside any previously described functional domains (except $TOR1^{WE}$ Phe1640 in the FAT domain). Three derived amino acid changes are unique to the $TOR2^{SA}$ allele (Glu122Gly, Ile1369Met, and Ile1872Leu) and all of them are predicted to be deleterious (supplementary table S7, Supplementary Material online).

To expand our understanding of natural genetic variation of these shared selection targets, we compared the sequences of *RNR4*, *TOR1*, and *TOR2* across >1,000 *S. cerevisiae* natural isolates (Peter et al. 2018). All the three genes are highly conserved (fig. 6) and we predicted 9, 79, and 73 amino acid sites of *RNR4*, *TOR1*, and *TOR2*, respectively, to be functionally important (supplementary table S8, Supplementary Material online). All the nine *RNR4* sites are in the ribonucleotide reductase domain in which the pre-existing and de novo driver variants are located. About 38.0% (30/79) of the amino acid changes in *TOR1* and 46.6% (34/73) in *TOR2* are located in known domains, including four *TOR1* and two *TOR2* substitutions in the RM-binding domain. We have experimentally confirmed that two of such pre-existing variants (*TOR1* His2000 and *TOR2* Leu2047) can confer RM resistant (supplementary fig. S5, Supplementary Material online).

Given that the *TOR1*, *TOR2* pre-existing and de novo variants coexist in the same population, we further investigated their potential interactions. We genotyped the local genetic

backgrounds of *TOR1* de novo mutants and found them to be heterogeneous (supplementary table S4, Supplementary Material online). This lack of interplay between *TOR1* mutations and their local genetic backgrounds is consistent with the background-independent emergence of *TOR1* mutations. Surprisingly, the *TOR2* mutation emerged in a clone carrying the weak $TOR2^{SA}$ allele. The frequency of $TOR2^{SA}$ initially dropped from 0.29 (T0) to 0.04 (T8). After being hijacked by the *TOR2* Ser1975Ile de novo mutation, its frequency abruptly increased to 0.46 (T15, supplementary fig. S10, Supplementary Material online). Thus, the emergence of the de novo *TOR2* mutation masked the RM-susceptibility of the weak $TOR2^{SA}$ background. One interpretation of this is that pre-existing and de novo *TOR* variants affect RM resistance via distinct mechanisms. The de novo mutation predominantly occurred in the RM binding domain and acted by impairing FKBP12-RM binding. We hypothesized that the pre-existing variants acted by providing higher basal TORC1 activity. This would maintain sufficient TORC1 activity despite a subset of complexes consistently being inactivated by FKBP12-RM binding. In contrast, the de novo mutations in the RM-binding domain were known not to affect TORC1 activity (González et al. 2015). To explore this, we measured the TORC1 activity of the *TOR1* and *TOR2* pre-existing variants by a highly specific antibody that assessed the phosphorylation of the ribosomal protein S6 (Rps6) under RM exposure (Supplementary notes). Rps6 phosphorylation is regulated by TORC1 and can therefore be used as a specific in vivo assay for TORC1 activity (González et al. 2015). Rps6 phosphorylation increased in the strains with the RM resistant $TOR1^{SA}$ and $TOR2^{WE}$ alleles (fig. 5*D*), indicating enhanced TORC1 activity. The enhanced TORC1 activity of $TOR1^{SA}$ and $TOR2^{WE}$ alleles is intriguing, especially considering a majority of the SNVs in these alleles occur outside known functional domains. Taken together, we conclude that the pre-existing and de novo variants converged to *TOR1* and *TOR2* for RM resistance but via distinct functional mechanisms.

Functional Consequences of TOR Natural Variants

TOR1 and *TOR2* are master regulators of growth with a shared role in forming TORC1, which is uniquely sensitive to RM (Loewith et al. 2002). We were particularly intrigued by the opposite RM resistance phenotypes of the SA and WE alleles of these two paralogous genes, as they occur in two independently domesticated lineages for alcoholic beverage production (Fay and Benavides 2005). We therefore characterized the *TOR1* and *TOR2* alleles from these two parental backgrounds to assess their respective impacts on fitness in environments of industrial and medical interest.

Given the role of TORC1 in regulating chronological life span (CLS) (Powers et al. 2006), we measured the impact of TOR variants on CLS (see Supplementary notes). In the presence of RM, clones with the $TOR1^{SA}$ and $TOR2^{WE}$ alleles conferred faster growth but shorter CLS than their counterparts with the $TOR1^{WE}$ and $TOR2^{SA}$ alleles (fig. 5*A*–*C*). The wild type hybrid WE/SA showed fastest growth and shortest CLS, indicating *TOR1* and *TOR2* haplo-insufficiency for growth but haplo-proficiency for CLS. In the absence of RM, there is almost no difference in CLS between strains, indicating that the haplo-proficient effect of single copy *TOR1* and *TOR2* has already saturated in rich medium.

Although RM is an unlikely selection pressure for natural yeast populations, real ecological constraints such as nitrogen limitation do affect cell growth via TOR-dependent pathways (Loewith and Hall 2011) and is of central importance for wine fermentation. To further explore the *TOR1*, *TOR2* allele preferences between the SA and WE backgrounds and to illuminate the underlying mechanism, we measured their effect on doubling time in 18 environments, including nitrogen-limitations and synthetic wine must (fig. 5*E*). As expected, the WE strain showed fastest growth in synthetic wine must, consistent with its niche-specific domestication history. In general, the removal of one *TOR* allele led to growth defects in nitrogen-limited environments, and the removal of the WE allele seemed more adverse than the removal of the SA allele. For example, hybrids carrying $TOR1^{WE}$ grew faster than those carrying $TOR1^{SA}$ on methionine and threonine; and hybrids with $TOR2^{WE}$ grew faster than those with $TOR2^{SA}$ in tryptophan, threonine, serine, methionine, isoleucine, asparagine, and adenine.

Taken together, the background-specific functional divergence of the WE and SA alleles on both *TOR1* and *TOR2* are not limited to RM resistance. Substantial differences are also found in many other biological traits such as TORC1 activity, chronological aging, and nitrogen-dependent growth, which further highlight the functional impact of the independent domestication histories of the WE and SA strains (Fay and Benavides 2005).

TOR2 Is a Conditionally Essential Gene

TOR2 has a unique role in forming TORC2, which is insensitive to RM (Loewith et al. 2002) and essential for the growth of the laboratory strain S288C (Winzeler et al. 1999; Liu et al. 2015). As expected, *TOR2* could not be deleted in WE, NA, or WA. However, we were surprisingly able to delete *TOR2* in the SA haploid. The *tor2*Δ SA strain can grow on synthetic complete medium (SC), although with severe growth defects, but not on YPD (fig. 7*A* and *B*). TORC1 activity of *tor2*Δ SA remained unaltered upon the RM treatment (fig. 7*C*), indicating that the SA background is able to compensate the *TOR2* loss and does not use *TOR2* in TORC1 at all. We dissected ~900 spores from WE/SA *TOR2* reciprocal hemizygous deletions (*tor2*Δ/*TOR2*), as well as WE/SA wild type on both YPD and SC medium. On SC, the spore viability is 83.5% for the wild type and 55.3% for the *tor2*Δ/*TOR2* cross. Therefore, *TOR2* is essential in a fraction of the recombined WE/SA offspring. By tracking the deletion marker, we estimated that 18.5% of the *tor2*Δ recombinants survived on SC (supplementary table S9, Supplementary Material online) despite growth defects (fig. 7*D*), whereas no *tor2*Δ spores can survive on YPD. Therefore, *TOR2* is conditionally essential, depending on both genetic backgrounds and growth conditions. We do not have an explicit answer for why the *tor2*Δ cells can grow on SC but not on YPD. A plausible explanation is the different amounts and types of nitrogen in SC and YPD,

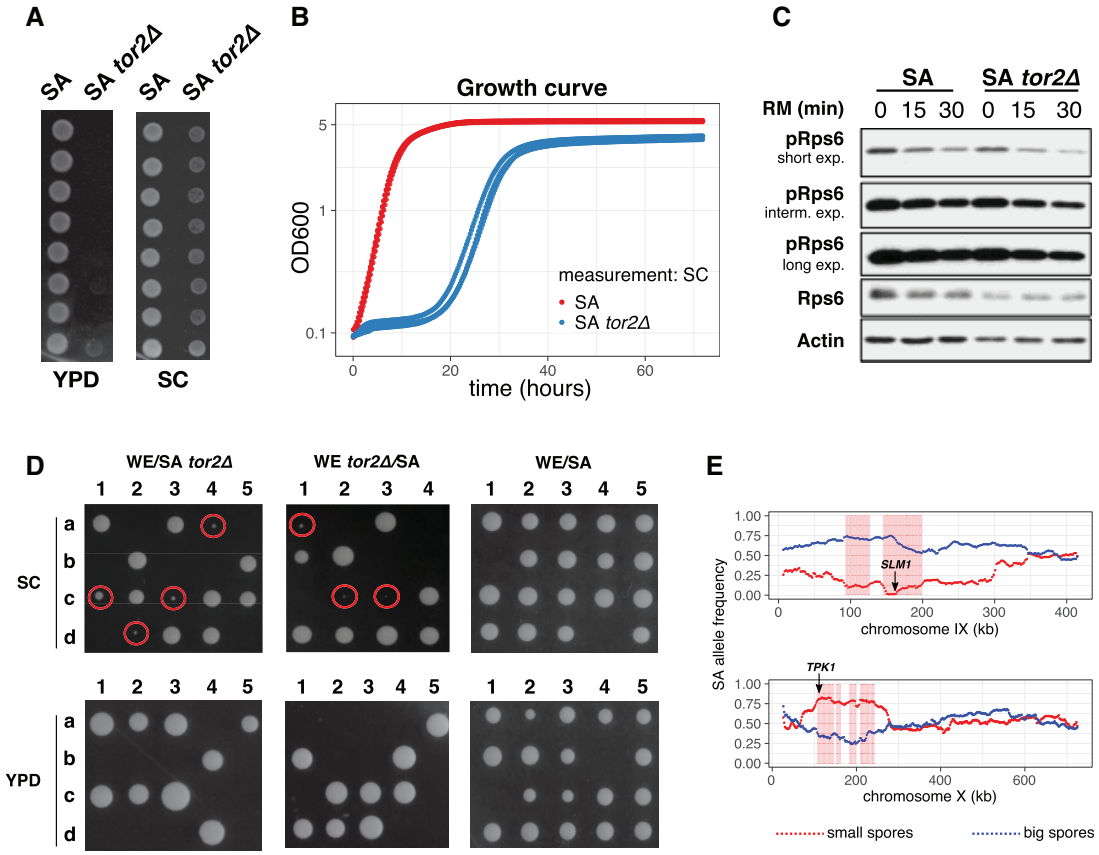

Fig. 7. Functional characterization of the *TOR2* variants. (*A*) The SA *tor2*Δ cells are able to grow on synthetic complete (SC) medium although with visible growth defect, but not on YPD. (*B*) Growth curves of the SA *tor2*Δ and SA wild type strains growing in SC measured by Tecan plate reader. (*C*) Immunoblot analysis showed Rps6 phosphorylation in SA wild type and *tor2*Δ strains. The TORC1 activity is not altered by the *TOR2* deletion. All the conditions are similar to the one reported in fig. 5*D*. (*D*) Representative plates acquired 4 days after tetrad dissection on SC and YPD for WE/SA wild type and its *TOR2* reciprocal hemizygotes. The red circles indicate viable *tor2*Δ strains. (*E*) The SA allele frequency on chromosome IX (top) and X (bottom) reveal the regions and candidate genes which compensate for the loss of *TOR2*. The red box highlights the regions with extremely high (99th percentile) or low (1st percentile) SA allele frequencies in the small spores. The coordinate is based on the WE reference (DBVPG6765, see Yue et al. 2017).

given that the key function of TOR is to signal the nitrogen status of the cell.

The conditional essentiality is usually regulated by complex genetic interactions, relying on multiple background-specific modifiers (Dowell et al. 2010). The tetrad segregation patterns suggest at least two unlinked loci contributing to the *TOR2* dispensability (supplementary table S10, Supplementary Material online). We genotyped the *TOR1* in the surviving *tor2*Δ spores to test if the $TOR1^{SA}$ could buffer the *TOR2* loss. However, only half of the *tor2*Δ spores had the $TOR1^{SA}$, suggesting that *TOR1* genotype on its own was not sufficient to rescue the *TOR2* deletion, although this did not exclude the possibility that *TOR1* participated in TORC2 by interacting with other modifiers. We also sequenced pools of *tor2*Δ and wild type spores to compare parental allele frequency changes and mapped regions with significant changes (Supplementary notes). We detected the regions on chromosome IX (163–178 kb) and X (106–134 kb) with significant difference in allele frequencies (fig. 7*E*). The chromosome X region peaks near *TPK1*, which responds to nutrients via the RAS-cAMP signaling pathway. The activation of this pathway suppresses the TOR deficiency (Schmelzle et al. 2004). The chromosome IX region contains *SLM1*, which regulates actin cytoskeleton organization, responds to stress and can be phosphorylated by TORC2. We expect the positive modifiers of *TOR2* dispensability to favor the SA background, which is the case for the *TPK1* locus. However, the *SLM1* was selected from the WE allele in WE/SA segregants, likely due to epistatic effects. These results indicate that the biological processes of rescuing *TOR2* loss are highly complex.

Discussion

We devised a unique experimental system with yeast populations derived from one, two, and four parental strains to quantify how varying levels of pre-existing variation affect evolutionary dynamics and to understand whether pre-existing and de novo variants are selected on shared molecular targets. We found that the doubling of the segregating genetic diversity alone raised the adaptive gain by >50% (51.5% in RM and 64.1% in HU) in the absence of de novo mutations. Therefore, the higher genetic heterogeneity translates into higher fitness variance, which is a prerequisite for faster adaptation. Our findings provide a starting point for placing the

evolutionary theory of pre-existing variation on a sound empirical basis.

Frequency dynamics of pre-existing variants in the four-parent populations revealed QTLs driving the early adaptation. The notably high number of QTLs (13 in RM and 9 in HU) vastly exceeded the single one mapped in the two-parent populations (*CTF8* in RM). The explanation to such clear difference is partially a matter of new alleles being available in the four-parent populations. For example, the largest effect QTLs (*RNR4*, *TOR1*, and *TOR2*) are driven by the WE and SA alleles that are absent in the two-parent populations. However, there are other QTLs corresponding to the WA and NA alleles but were only observed in the four-parent populations, highlighting the dependence of complex epistatic interactions on higher genetic heterogeneity (Burke et al. 2010).

Towards the later phase of our selection experiment, highly resistant clones emerged and rose to high frequency in both HU and RM. Nevertheless, the genetic origin and make-up of these clones differ dramatically between these two selection regimes. Pre-existing variants appeared to drive HU adaptation all the way to the end, implying that beneficial de novo mutations are either too rare or less fit than the bulk dynamics driven by the pre-existing beneficial alleles (i.e., the nine QTLs), which in fact is evident from the higher fitness of the final four-parent populations evolved in HU than that of the two-parent and NA populations acquiring *RNR* mutations (fig. 1C). Understanding the mechanisms behind require further work, which could be tested experimentally by lineage tracing or competition experiments. It could also be partially explained by negative or sign epistasis weakening the effects of beneficial de novo alleles (Khan et al. 2011). An additional explanation is that the *RNR* driver mutations appear to be strongly background-dependent. This is manifested by the two batches of experimental evolution in HU, revealing that *RNR* mutations are much easier to acquire in the background of homozygous NA or heterozygous NA × WA than that of homozygous SA, WE, or WA. Also, we cannot rule out the adaptive variants other than point mutations, such as structural rearrangements, but these are difficult to detect using short-read sequencing in bulk. In contrast, the mid to late adaptation to RM was consistently driven by clones with de novo mutations in *TOR1*, *TOR2*, and *FPR1* that emerged and overtook the other competing bulk subpopulations. This is consistently true in all genetic contexts and at all levels of pre-existing variation. We also frequently observed that the homozygous mutations acquired by the second hit of LOH to be more adapted than their heterozygous counterparts. LOH is commonly observed in many cancer types, which usually inactivate the function of tumor suppressor genes (Ryland et al. 2015). These indicate an important role of LOH in promoting clonal evolution and thus influencing the dynamics of cancer development and treatment (Ford et al. 2015; Vázquez-García et al. 2017).

Our work provides the first example of shared selection targets between pre-existing and de novo variants. The convergent selection on both pre-existing and de novo variants of *TOR1* and *TOR2* is particularly intriguing. First, strong loss-of-function de novo variants often play an outsized role in adaptation to a single constrained selective pressure. However, such mutations are not likely to prevail in natural populations that experience changing environments, because purifying selection acts to remove deleterious variants (Bamshad and Wooding 2003). Second, many pre-existing variants from the natural population may not show up as de novo mutations because the underlying mutation events are too rare. More interestingly, we found that the de novo and pre-existing variants confer RM resistance via distinct mechanisms: abolishing drug binding by de novo variants (Loewith and Hall 2011) and altering the TORC1 activity by pre-existing variants. This mechanistic distinction has been supported by the immunoblotting of the *TOR1/2* reciprocal hemizygotes and the fact that a driver mutation in the drug-binding domain can completely rescue the nearly extinct weak $TOR2^{SA}$ allele with low TORC1 activity (supplementary fig. S10, Supplementary Material online). This distinction suggests that the drug-binding domain is under consistent purifying selection, whereas TORC1 activity is under no or sub-population specific selection. Moreover, the *TOR2* de novo mutation is much rarer (only one single instance among all the isogenic, two-parent, and four-parent populations) despite the fact that its drug-binding domain has a similar target size as *TOR1* and that *TOR1* and *TOR2* are thought to be functionally redundant in RM resistance (Loewith and Hall 2011). The most likely explanation for this drastic difference is the stronger selection constraint on *TOR2*, which reflects its unique and essential role in forming the TORC2 complex.

The pre-existing WE and SA variants of the two *TOR* paralogs show opposite effects on RM resistance, reflecting lineage-specific functional divergence following the *TOR* gene duplication. Domestication to industrial niches with distinct substrates of fermentation (grape-wine and sake) (Giudici and Zambonelli 1992; Sasaki et al. 2014) may be one of the explanations for this functional divergence with drug resistance as a side-effect caused by the TOR pleiotropy. Finally, recent studies have implicated intratumoral heterogeneity as a significant driver of drug resistance, bearing big challenges to chemotherapy (Saunders et al. 2012). Both the acceleration of adaptation by higher pre-existing variation, and the shared targets between pre-existing and de novo variants observed in this study have important implications in our understanding of drug resistance evolution and treatment development (McGranahan and Swanton 2017).

Materials and Methods

Experimental Evolution and Genome Sequencing

All the strains used in this study are listed in supplementary table S11, Supplementary Material online. We previously generated two F12 populations (four-parent populations—F12_1 and F12_2) via the independent intercrosses of four diverged parental strains: DBVPG6044 (West Africa, "WA"), DBVPG6765 (Wine European, "WE"), Y12 (Sake, "SA"), and YPS128 (North America, "NA") (Cubillos et al. 2013). The experimental evolution was initiated from random subsamples of F12_1 and F12_2 with population size of 10^7–10^8 cells.

In parallel, experimental evolution was also initiated from isogenic parental populations of similar size. Cells were evenly spread on YPD agar plates (2% peptone, 1% yeast extract, 2% glucose, 2% agar) with HU (10 mg/ml) or RM (0.025 μg/ml), and incubated at 23°C (of note, we used 23°C instead of 30°C to avoid selection against WA alleles given this background is very sensitive to high temperature). Every 2–3 days, all the cells were collected from each plate and resuspended in 1 ml of distilled water. Ten percent of the cell suspension was plated to a new plate, whereas the remaining 90% were kept in 25% glycerol at −80°C. The selection experiment lasted for 32 days and an overview of the timeline and populations is reported in supplementary tables S1 and S2, Supplementary Material online. For each drug, there are four independently evolving replicates derived from F12_1 and F12_2 respectively, as well as five or two replicates for each of the parental isogenic populations in HU or RM, respectively. An additional 15 clones (with three replicates each) from the two-parent populations with different levels of HU tolerance evolved in HU similarly as described above. We also propagated two replicates derived from F12_1 and F12_2 respectively using drug-free YPD as the control. Procedures were identical to those used for generating and evolving the previously published two-parent population (Vázquez-García et al. 2017). DNA was extracted from populations of T0, T1, T2, T4, T8, and the last time point (T14 or T15) using "Yeast MasterPure" kit (Epicentre, USA). All samples were sequenced using paired-end sequencing on Illumina HiSeq 2000/2500 (with Illumina TruSeq SBS v4 chemistry) at the Wellcome Trust Sanger Institute (Cambridge, United Kingdom).

Sequence Alignment, Genotype Calling of Pre-existing Variants and Detection of De Novo Mutations

The sequencing reads were aligned to the *S. cerevisiae* S288C reference genome (Release R64-1-1). Sequence alignment was carried out with Stampy v1.0.23 (Lunter and Goodson 2011) and local realignment using BWA v0.7.12 (Li and Durbin 2009). We used SAMtools v1.2 (Li 2011) to count read numbers covering each segregating site (Cubillos et al. 2013) and estimated the parental allele frequency accordingly. We performed de novo mutation calling for each sequenced sample using three different algorithms: GATK 2.1-5-gf3daab0 (DePristo et al. 2011), Platypus v0.7.9.1 (Rimmer et al. 2014), and SAMtools v1.2 (Li 2011). We then filtered these calls by subtracting all variation called from the parental samples to remove pre-existing variants, required each variant to be on a locus with >10 reads in total and >6 reads reporting the variant allele, and to pass default filters of the algorithms. For Platypus, we included allele bias flagged calls as the sequenced samples are pools and therefore can have a range of variant allele fractions. We then intersected the calls and filtered out those variants called by only one variant caller. For the confirmed driver mutations at the end time point, we further examined their frequency across all previous time points. Finally, we used Ensembl Variant Effect Predictor (VEP) to annotate the mutations (McLaren et al. 2016).

Estimating Allele Frequencies

We define the allele frequency x_i^j at locus i of an allele j in the cross, for example, we define x_i^{WA} to refer to the frequency of the WA allele at locus i (and so on for $j \in \{\text{WA, NA, WE, SA}\}$). The allele frequency at locus i is normalized, such that $x_i^{WA} = 1 - \sum_{j\in\{NA,\ WE,\ SA\}} x_i^j$. Given the number of reads n_i^j mapping to each allele and the total number of reads at each segregating locus, we estimated the allele frequency using the filterHD algorithm (Fischer et al. 2014). filterHD fits a jump-diffusion process to the data where the diffusion component models the persistence of allele frequencies along the genome, reflecting linkage disequilibrium of nearby loci. Conversely, the jump component allows sudden changes in the allele frequency, which reflects the genotype state of large clones in populations that became clonal during the experiment.

Estimating Copy Number Variation

The per-base sequencing depth was calculated by SAMtools v1.2 (Li 2011), which were further used to calculate the median sequencing depth (x) for each chromosome.

Mapping QTLs

Given our allele frequency estimates, we used a 10-kb sliding window with a 2-kb step size to localize QTLs. For each heterogeneous population, we compared the allele frequency change in a window i between time point t and T0 (e.g., $\Delta x_i^j(t) = x_i^j(t) - x_i^j(0), \quad j = \{\text{WA, NA, WE, SA}\}$). If there is selection on pre-existing variants, we expect a steady increase of favored parental allele frequency in regions under selection as selection proceeds. Therefore, for each early transfer, we calculated the z-score of allele frequency changes compared with T0 in each population: $z_{\Delta x} = (\Delta x_i^j - \mu_{\Delta x})/\sigma_{\Delta x}$. Here, $\mu_{\Delta x}$ and $\sigma_{\Delta x}$ are the mean and standard deviation of Δx_i^j in all the four-parent populations evolved in the drug at a certain time point. The z-score square reflects the allele frequency deviation from T0. Given the fact that we observed dominant clones at the later phase of our experiment, we only used the early phase to map QTLs: T0—T4 for HU and T0—T2 for RM. This timing cut-off is determined by the patterns of allele frequency distribution (supplementary fig. S7, Supplementary Material online). Without dominant clone(s), the allele frequency distribution of the four parental lineages should follow a normal distribution with mean of ~0.25. When dominant clones emerge and deplete the genetic heterogeneity of the population, the distribution pattern should change dramatically, resulting strong allele frequency deviation from 0.25. We searched for regions with z-score square higher than 99% or 95% quantile for each early time point. If the examined regions pass these cut-offs across T1—T2 for RM and across T1—T4 for HU, but not in the control (drug-free condition), they are assumed to be QTLs (fig. 4A and supplementary fig. S9 and table S5, Supplementary Material online). We excluded regions located near chromosome ends, which are prone to false positives due to the rich repetitive sequence content. Using this method, we also reanalyzed the data from our previous two-parent population experiment to make sure that the

contrasting numbers of QTLs identified from the four-parent and two-parent populations are not due to methodology artifact. QTLs could be either maintained until later time points or be hijacked by the spread of clones with beneficial de novo mutations. We define whether a QTL is maintained by counting the replicates in which the strong allele keeps increasing or the weak allele keeps decreasing until T4, T8 and the end. If the number of such replicates is more than six (eight replicates in total), we defined the QTL as maintained until the later time points (supplementary fig. S8 and tables S5 and S6, Supplementary Material online).

Growth Phenotyping

Quantitative Measurement

For phenotyping, we sampled the bulk from the isogenic, two-parent and four-parent populations at each serial transfer of the experimental evolution (supplementary table S1, Supplementary Material online), thousands of randomly isolated clones from initial and final populations (supplementary table S2, Supplementary Material online), as well as strains with gene deletion (supplementary table S11, Supplementary Material online). Using a high-resolution large-scale scanning platform, Scan-o-matic, we monitored growth in a 1536-colony design on solid agar plate (Zackrisson et al. 2016). The Scan-o-matic program uses the data from the images taken by the high-quality desktop scanners to calculate the population size and generate growth curves for the colonies. All the scripts are available on GitHub (https://github.com/Scan-o-Matic/scanomatic; last accessed February 3, 2019). Downstream analysis of doubling time acquired by Scan-o-matic was performed using R and scripts are available on GitHub (see Data availability). The scanners monitored the colonies growth on synthetic complete (SC) medium (0.14% YNB, 0.5% ammonium sulfate, 0.077% Complete Supplement Mixture [CSM, ForMedium], 2% (w/v) glucose and pH buffered to 5.8 with 1% (w/v) succinic acid) with drugs (10 mg/ml HU, 0.025 μg/ml RM), and without drug as control at 30°C. We used SC medium rather than YPD because (1) YPD does not allow transmissive scanning due to light scattering; (2) SC medium is more homogeneous than YPD across the plate; (3) YPD medium has limited buffering capacity, which is a major issue in a colony-based agar screen because of the interaction of neighboring colonies through the acidic metabolites secreted as they expand. Such interactions lead to large position-dependent biases that are difficult to account for. The SC medium is buffered to pH 5.8, dramatically reducing acidity gradients across the plate due to secreted metabolites. Therefore, these conditions are optimized for phenotyping and the noise due to variation in temperature and medium composition between the experimental evolution and phenotyping condition is negligible (Warringer et al. 2011). The nitrogen-limited medium used to test the TOR variants contains a single nitrogen source present at 30 mg nitrogen/l (Ibstedt et al. 2015). Experiments were run for 3 days and scans were continuously performed every 20 min. After quality control filtering, the measurement of doubling time was extracted for downstream analysis in R (R version 3.4.1). All custom R scripts used for making the plots are available via the GitHub project repository (see Data availability). Multiple technical replicates (n) were applied during phenotyping: $n \geq 8$ for each sample in drug condition; $n \geq 2$ in drug-free condition; $n \geq 96$ for the samples phenotyped in nitrogen-limited conditions. We reported the error of technical replicates by listing the standard deviation (SD) in supplementary table S12, Supplementary Material online.

We also used the Tecan Infinite 200 PRO plate reader to measure growth curves in small scale. We precultured the cells overnight and diluted the saturated culture 100 times into fresh medium. We measured OD_{600} every 15 min for at least 3 days in drugs and control. The raw OD_{600} values were corrected and then used to generate growth curves. Doubling time and yield were extracted using the online tool "PRECOG" (Fernandez-Ricaud et al. 2016). Of note, Scan-o-matic is the predominant phenotyping method in this study and we notified explicitly in the figure legend if Tecan plate reader was used for phenotyping.

Qualitative Measurement

We performed serial dilution and spotting of the cells to visually assess adaptation at the population level (supplementary fig. S1, Supplementary Material online) as well as the growth phenotypes of gene deletions (supplementary fig. S5, Supplementary Material online). Cells were precultured in YPD overnight to saturation. Then 5 µl of the culture was taken for spotting assay in the condition of interest. There were a total of six 1:10 dilutions from left to right on the plate. We also conducted spotting assay for 48 isolates drawn from the SA population evolved in RM (SA_RM_2_T15) in heat condition (40 °C). For these isolates, we precultured cells in YPD overnight. Then 5 µl cells of 1,000-fold dilution from saturation were taken to put on YPD and incubated at 40 °C. The plates were scanned after two days.

Statistical Analysis

The Mann–Whitney U test was performed in R using the *wilcox.test ()* function, with two-sided alternative hypothesis. Unless otherwise stated, the doubling time mentioned in the text corresponds to the mean value of indicated samples.

Data Availability

The source data files and custom scripts are provided in the GitHub project repository via the following link: https://github.com/lj1221/four_parent_experimental_evolution_2017, last accessed February 3, 2019.

More details of the 1002 Yeast Genome Project are available via the link: http://1002genomes.u-strasbg.fr/, last accessed February 3, 2019.

Sequence data is deposited to NCBI SRA database with BioProject accession number PRJEB4645.

Additional details of materials and methods are included in the Supplementary notes.

Supplementary Material

Supplementary data are available at *Molecular Biology and Evolution* online.

Acknowledgments

We thank Johan Hallin for critical reading of the manuscript. This research is supported by ATIP-Avenir (CNRS/INSERM), Fondation ARC (grant number SFI20111203947), FP7-PEOPLE-2012-CIG (grant number 322035), the French National Research Agency (grant number ANR-13-BSV6-0006-01), Cancéropôle PACA (AAP emergence), and DuPont Young Professor Award to G.L., by the Wellcome Trust to I.V.-G. (grant number WT097678) and to V.M. (grant number WT098051), by the Swedish Research Council (grant numbers 325-2014-6547 and 621- 2014-4605) to J.W. J.L. is supported by Fondation ARC pour la Recherche sur le Cancer (grant number PDF20140601375). J.-X.Y. is supported by Fondation ARC pour la Recherche sur le Cancer (PDF20150602803). B.B. was supported by La Ligue Contre le Cancer (grant number GB-MA-CD-11287) and Fondation pour la Recherche Médicale (FDT20170437209). We also acknowledge CytoMed, the IRCAN Flow Cytometry Facility and the Genomics Core Facility. The materials of CytoMed were supported by the Conseil Général 06, the FEDER, the Ministère de l'Enseignement Supérieur, the Région Provence Alpes-Côte d'Azur, and the INSERM.

References

Bamshad M, Wooding SP. 2003. Signatures of natural selection in the human genome. *Nat Rev Genet*. 4(2):99.

Barrett RDH, Schluter D. 2008. Adaptation from standing genetic variation. *Trends Ecol Evol*. 23(1):38–44.

Barrick JE, Yu DS, Yoon SH, Jeong H, Oh TK, Schneider D, Lenski RE, Kim JF. 2009. Genome evolution and adaptation in a long-term experiment with Escherichia coli. *Nature* 461(7268):1243–1247.

Berg JJ, Coop G. 2015. A coalescent model for a sweep of a unique standing variant. *Genetics* 201(2):707–725.

Burke MK, Dunham JP, Shahrestani P, Thornton KR, Rose MR, Long AD. 2010. Genome-wide analysis of a long-term evolution experiment with Drosophila. *Nature* 467(7315):587–590.

Burke MK, Liti G, Long AD. 2014. Standing genetic variation drives repeatable experimental evolution in outcrossing populations of *Saccharomyces cerevisiae*. *Mol Biol Evol*. 31(12):3228–3239.

Cafferkey R, Young PR, McLaughlin MM, Bergsma DJ, Koltin Y, Sathe GM, Faucette L, Eng WK, Johnson RK, Livi GP. 1993. Dominant missense mutations in a novel yeast protein related to mammalian phosphatidylinositol 3-kinase and VPS34 abrogate rapamycin cytotoxicity. *Mol Cell Biol*. 13(10):6012–6023.

Cubillos FA, Louis EJ, Liti G. 2009. Generation of a large set of genetically tractable haploid and diploid Saccharomyces strains. *FEMS Yeast Res*. 9(8):1217–1225.

Cubillos FA, Parts L, Salinas F, Bergström A, Scovacricchi E, Zia A, Illingworth CJR, Mustonen V, Ibstedt S, Warringer J, et al. 2013. High-resolution mapping of complex traits with a four-parent advanced intercross yeast population. *Genetics* 195(3):1141–1155.

DePristo MA, Banks E, Poplin R, Garimella KV, Maguire JR, Hartl C, Philippakis AA, Angel G, del Rivas MA, Hanna M, et al. 2011. A framework for variation discovery and genotyping using next-generation DNA sequencing data. *Nat Genet*. 43(5):491–498.

Dowell RD, Ryan O, Jansen A, Cheung D, Agarwala S, Danford T, Bernstein DA, Rolfe PA, Heisler LE, Chin B, et al. 2010. Genotype to phenotype: a complex problem. *Science* 328(5977):469.

Fay JC, Benavides JA. 2005. Evidence for domesticated and wild populations of *Saccharomyces cerevisiae*. *PLoS Genet* 1(1):e5.

Fernandez-Ricaud L, Kourtchenko O, Zackrisson M, Warringer J, Blomberg A. 2016. PRECOG: a tool for automated extraction and visualization of fitness components in microbial growth phenomics. *BMC Bioinformatics* 17:249.

Fischer A, Vázquez-García I, Illingworth CJR, Mustonen V. 2014. High-definition reconstruction of clonal composition in cancer. *Cell Rep*. 7(5):1740–1752.

Ford CB, Funt JM, Abbey D, Issi L, Guiducci C, Martinez DA, Delorey T, Li B, yu White TC, Cuomo C, et al. 2015. The evolution of drug resistance in clinical isolates of Candida albicans. *eLife* 4:e00662.

Gerrish PJ, Lenski RE. 1998. The fate of competing beneficial mutations in an asexual population. *Genetica* 102–103:127–144.

Giudici P, Zambonelli C. 1992. Biometric and genetic study on acetic acid production for breeding of wine yeast. *Am J Enol Vitic*. 43:370–374.

Gjuvsland AB, Zörgö E, Samy JK, Stenberg S, Demirsoy IH, Roque F, Maciaszczyk-Dziubinska E, Migocka M, Alonso-Perez E, Zackrisson M, et al. 2016. Disentangling genetic and epigenetic determinants of ultrafast adaptation. *Mol Syst Biol*. 12(12):892.

González A, Shimobayashi M, Eisenberg T, Merle DA, Pendl T, Hall MN, Moustafa T. 2015. TORC1 promotes phosphorylation of ribosomal protein S6 via the AGC kinase Ypk3 in *Saccharomyces cerevisiae*. *PLoS One* 10(3): e0120250.

Heitman J, Movva NR, Hall MN. 1991. Targets for cell cycle arrest by the immunosuppressant rapamycin in yeast. *Science* 253(5022):905–909.

Helliwell SB, Wagner P, Kunz J, Deuter-Reinhard M, Henriquez R, Hall MN. 1994. TOR1 and TOR2 are structurally and functionally similar but not identical phosphatidylinositol kinase homologues in yeast. *Mol Biol Cell*. 5(1):105–118.

Hermisson J, Pennings PS. 2005. Soft sweeps. *Genetics* 169(4):2335–2352.

Herron MD, Doebeli M. 2013. Parallel evolutionary dynamics of adaptive diversification in *Escherichia coli*. *PLoS Biol*. 11(2): e1001490.

Ibstedt S, Stenberg S, Bagés S, Gjuvsland AB, Salinas F, Kourtchenko O, Samy JKA, Blomberg A, Omholt SW, Liti G, et al. 2015. Concerted evolution of life stage performances signals recent selection on yeast nitrogen use. *Mol Biol Evol*. 32(1):153–161.

Khan AI, Dinh DM, Schneider D, Lenski RE, Cooper TF. 2011. Negative epistasis between beneficial mutations in an evolving bacterial population. *Science* 332(6034):1193–1196.

Kosheleva K, Desai MM. 2018. Recombination alters the dynamics of adaptation on standing variation in laboratory yeast populations. *Mol Biol Evol*. 35(1):180–201.

Kvitek DJ, Sherlock G. 2013. Whole genome, whole population sequencing reveals that loss of signaling networks is the major adaptive strategy in a constant environment. *PLoS Genet*. 9(11): e1003972.

Lang GI, Rice DP, Hickman MJ, Sodergren E, Weinstock GM, Botstein D, Desai MM. 2013. Pervasive genetic hitchhiking and clonal interference in forty evolving yeast populations. *Nature* 500(7464):571–574.

Levy SF, Blundell JR, Venkataram S, Petrov DA, Fisher DS, Sherlock G. 2015. Quantitative evolutionary dynamics using high-resolution lineage tracking. *Nature* 519(7542):181–186.

Li H. 2011. A statistical framework for SNP calling, mutation discovery, association mapping and population genetical parameter estimation from sequencing data. *Bioinformatics* 27(21):2987–2993.

Li H, Durbin R. 2009. Fast and accurate short read alignment with Burrows-Wheeler transform. *Bioinformatics* 25:1754–1760.

Liu G, Yong MYJ, Yurieva M, Srinivasan KG, Liu J, Lim JSY, Poidinger M, Wright GD, Zolezzi F, Choi H, et al. 2015. Gene essentiality is a quantitative property linked to cellular evolvability. *Cell* 163(6):1388–1399.

Loewith R, Hall MN. 2011. Target of rapamycin (TOR) in nutrient signaling and growth control. *Genetics* 189(4):1177–1201.

Loewith R, Jacinto E, Wullschleger S, Lorberg A, Crespo JL, Bonenfant D, Oppliger W, Jenoe P, Hall MN. 2002. Two TOR complexes, only one of which is rapamycin sensitive, have distinct roles in cell growth control. *Mol Cell* 10(3):457–468.

Long A, Liti G, Luptak A, Tenaillon O. 2015. Elucidating the molecular architecture of adaptation via evolve and resequence experiments. *Nat Rev Genet*. 16(10):567–582.

Lunter G, Goodson M. 2011. Stampy: a statistical algorithm for sensitive and fast mapping of Illumina sequence reads. *Genome Res*. 21(6):936–939.

Mason DL, Mallampalli MP, Huyer G, Michaelis S. 2003. A region within a lumenal loop of *Saccharomyces cerevisiae* Ycf1p directs proteolytic processing and substrate specificity. *Eukaryot Cell* 2(3):588–598.

McGranahan N, Swanton C. 2017. Clonal heterogeneity and tumor evolution: past, present, and the future. *Cell* 168(4):613–628.

McLaren W, Gil L, Hunt SE, Riat HS, Ritchie GRS, Thormann A, Flicek P, Cunningham F. 2016. The ensembl variant effect predictor. *Genome Biol*. 17:122.

Palmer AC, Kishony R. 2013. Understanding, predicting and manipulating the genotypic evolution of antibiotic resistance. *Nat Rev Genet*. 14(4):243–248.

Parts L, Cubillos FA, Warringer J, Jain K, Salinas F, Bumpstead SJ, Molin M, Zia A, Simpson JT, Quail MA, et al. 2011. Revealing the genetic structure of a trait by sequencing a population under selection. *Genome Res*. 21(7):1131–1138.

Payen C, Sunshine AB, Ong GT, Pogachar JL, Zhao W, Dunham MJ. 2016. High-throughput identification of adaptive mutations in experimentally evolved yeast populations. *PLoS Genet*. 12(10): e1006339.

Peter J, Chiara MD, Friedrich A, Yue J-X, Pflieger D, Bergström A, Sigwalt A, Barre B, Freel K, Llored A, et al. 2018. Genome evolution across 1,011 *Saccharomyces cerevisiae* isolates. *Nature* 556(7701):339–344.

Powers RW, Kaeberlein M, Caldwell SD, Kennedy BK, Fields S. 2006. Extension of chronological life span in yeast by decreased TOR pathway signaling. *Genes Dev*. 20(2):174–184.

Rimmer A, Phan H, Mathieson I, Iqbal Z, Twigg SRF, Consortium W, Wilkie AOM, McVean G, Lunter G. 2014. Integrating mapping-, assembly- and haplotype-based approaches for calling variants in clinical sequencing applications. *Nat Genet*. 46(8):912–918.

Ryland GL, Doyle MA, Goode D, Boyle SE, Choong DYH, Rowley SM, Li J, Australian Ovarian Cancer Study Group, Bowtell DDL, Tothill RW. 2015. Loss of heterozygosity: what is it good for? *BMC Med Genomics* 8:45.

Sasaki K, Tsuge Y, Sasaki D, Hasunuma T, Sakamoto T, Sakihama Y, Ogino C, Kondo A. 2014. Optimized membrane process to increase hemicellulosic ethanol production from pretreated rice straw by recombinant xylose-fermenting *Saccharomyces cerevisiae*. *Bioresour Technol*. 169:380–386.

Saunders NA, Simpson F, Thompson EW, Hill MM, Endo -Munoz L, Leggatt G, Minchin RF, Guminski A. 2012. Role of intratumoural heterogeneity in cancer drug resistance: molecular and clinical perspectives. *EMBO Mol Med*. 4(8):675–684.

Schmelzle T, Beck T, Martin DE, Hall MN. 2004. Activation of the RAS/cyclic AMP pathway suppresses a TOR deficiency in yeast. *Mol Cell Biol*. 24(1):338–351.

Sheng Z, Pettersson ME, Honaker CF, Siegel PB, Carlborg Ö. 2015. Standing genetic variation as a major contributor to adaptation in the Virginia chicken lines selection experiment. *Genome Biol*. 16:219.

Stan R, McLaughlin MM, Cafferkey R, Johnson RK, Rosenberg M, Livi GP. 1994. Interaction between FKBP12-rapamycin and TOR involves a conserved serine residue. *J Biol Chem*. 269(51):32027–32030.

Teotónio H, Chelo IM, Bradić M, Rose MR, Long AD. 2009. Experimental evolution reveals natural selection on standing genetic variation. *Nat Genet*. 41(2):251–257.

Turner NC, Reis-Filho JS. 2012. Genetic heterogeneity and cancer drug resistance. *Lancet Oncol*. 13(4): e178–e185.

Vázquez-García I, Salinas F, Li J, Fischer A, Barré B, Hallin J, Bergström A, Alonso-Perez E, Warringer J, Mustonen V, et al. 2017. Clonal heterogeneity influences the fate of new adaptive mutations. *Cell Rep*. 21(3):732–744.

Venkataram S, Dunn B, Li Y, Agarwala A, Chang J, Ebel ER, Geiler-Samerotte K, Hérissant L, Blundell JR, Levy SF, et al. 2016. Development of a comprehensive genotype-to-fitness map of adaptation-driving mutations in yeast. *Cell* 166(6):1585–1596.e22.

Warringer J, Liti G, Blomberg A. 2017. Yeast reciprocal hemizygosity to confirm the causality of a quantitative trait loci-associated gene. *Cold Spring Harb Protoc*. 2017(8): pdb.prot089078.

Warringer J, Zörgö E, Cubillos FA, Zia A, Gjuvsland A, Simpson JT, Forsmark A, Durbin R, Omholt SW, Louis EJ, et al. 2011. Trait variation in yeast is defined by population history. *PLoS Genet*. 7(6): e1002111.

Winzeler EA, Shoemaker DD, Astromoff A, Liang H, Anderson K, Andre B, Bangham R, Benito R, Boeke JD, Bussey H, et al. 1999. Functional characterization of the *S. cerevisiae* genome by gene deletion and parallel analysis. *Science* 285(5429):901–906.

Yue J-X, Li J, Aigrain L, Hallin J, Persson K, Oliver K, Bergström A, Coupland P, Warringer J, Lagomarsino MC, et al. 2017. Contrasting evolutionary genome dynamics between domesticated and wild yeasts. *Nat Genet*. 49(6):913–924.

Zackrisson M, Hallin J, Ottosson L-G, Dahl P, Fernandez-Parada E, Ländström E, Fernandez-Ricaud L, Kaferle P, Skyman A, Stenberg S, et al. 2016. Scan-o-matic: high-resolution microbial phenomics at a massive scale. *G3 GenesGenomesGenetics* 6(9):3003–3014.